JOURNAL OF SOLID STATE CHEMISTRY **125,** 234–242 (1996)
ARTICLE NO. 0291

Hydrothermal Investigation of the Barium/Molybdenum(VI)/Selenium(IV) Phase Space: Single-Crystal Structures of $BaMoO_3SeO_3$ and $BaMo_2O_5(SeO_3)_2$

William T. A. Harrison,[1] Laurie L. Dussack, and Allan J. Jacobson[2]

Department of Chemistry, University of Houston, Houston, Texas 77204-5641

Received March 21, 1995; in revised form May 31, 1995; accepted June 5, 1996

The barium/molybdenum(VI)/selenium(IV)/oxide phase space has been investigated using hydrothermal methods. The syntheses and crystal structures of $BaMoO_3SeO_3$ and $BaMo_2O_5(SeO_3)_2$ are reported. Spectroscopic and thermogravimetric data for these phases are described. $BaMoO_3SeO_3$ is a layered compound, built up from "4-rings" of vertex-sharing MoO_6 and SeO_3 groups, linked into infinite, puckered sheets. Ten-coordinate Ba^{2+}species provide interlayer charge compensation. The distorted MoO_6 octahedron in $BaMoO_3SeO_3$ shows an unusual three short + three long Mo–O bond-distance distribution. Crystal data: $BaMoO_3SeO_3$, M_r = 408.23, monoclinic, space group $P2_1/c$ (No. 14), a = 6.242(3)Å, b = 10.192(3)Å, c = 8.373(2)Å, β = 94.94(3)°, V = 530.6(3)Å^3, Z = 4, $R(F)$ = 2.87%, $R_w(F)$ = 3.82% [1653 reflections with $I > 3\sigma(I)$]. $BaMo_2O_5(SeO_3)_2$ is a three-dimensional phase with respect to Mo–O–Mo and Mo–O–Se connectivity. Isolated, vertex-sharing pairs of MoO_6 octahedra are linked into a continuous network by pyramidal selenium atoms (as SeO_3^{2-} selenite ions). The MoO_6 octahedra in $BaMo_2O_5(SeO_3)_2$ display a typical two short + two intermediate + two long Mo–O bond-distance distribution. Ten-coordinate barium cations provide charge compensation. Crystal data: $BaMo_2O_5(SeO_3)_2$, M_r = 663.13, orthorhombic, space group $Cmc2_1$ (No. 36), a = 15.883(4)Å, b = 7.887(2)Å, c = 7.780(2)Å, V = 974.5(4)Å^3, Z = 4, $R(F)$ = 2.22%, $R_w(F)$ = 2.65% [943 reflections with $I > 3\sigma(I)$].

INTRODUCTION

We have recently described the hydrothermal syntheses and crystal structures of a large family of layered phases (1–8) whose structures are based on a single sheet of the hexagonal tungsten oxide (HTO) motif of corner-sharing octahedra (9). Of particular note here are the alkali metal/ammonium molybdenum selenites, $M_2(MoO_3)_3SeO_3$, with M = Cs, NH_4, Rb, or Tl (2, 8). These isostructural, non-centrosymmetric phases contain infinite layers of vertex-sharing MoO_6 groups, which form a network of three rings and six rings. Selenium atoms (as pyramidal $[SeO_3]^{2-}$ selenite anions) cap three-rings on one face of the Mo/O sheets. The extra-sheet univalent cations provide charge compensation for the anionic $(MoO_3)_3SeO_3$ layers.

We are now exploring the solid-state chemistry of molybdenum(VI), selenium(IV), and oxygen in combination with alkaline earth cations. In this paper we describe the results of exploratory hydrothermal synthesis in the barium/molybdenum(VI)/selenium(IV)/oxygen (Ba/Mo/Se/O) phase space. The new phases $BaMoO_3SeO_3$ and $BaMo_2O_5(SeO_3)_2$ have been prepared as single crystals and structurally characterized by X-ray diffraction.

EXPERIMENTAL

Hydrothermal Syntheses

The $Ba/Mo^{VI}/Se^{IV}/O/H_2O$ phase space was explored as a function of initial composition, temperature, and pH. Hydrothermal reactions were carried out at autogenous pressures in 23-mL capacity Teflon-lined stainless steel Parr hydrothermal bombs, with heating conditions as noted below. The solid reaction products were recovered by vacuum filtration and washing with water. All the phases recovered from this system are air stable. The approximate composition regions where the various phases were recovered and subsequently identified are mapped on a three-component mixture diagram (Fig. 1).

Transparent, platy, single crystals (to ~0.05 × 0.5 × 0.8 mm) of $BaMoO_3SeO_3$ were prepared from the reaction of 0.6855 g $BaCO_3$ (3.474 mmol Ba), 0.50 g MoO_3 (3.474 mmol Mo), 0.771 g SeO_2 (6.95 mmol Se), and 10 cm^3 deionized water (Ba : Mo : Se ratio = 1 : 1 : 2). These reactants were sealed into a Parr bomb and heated to 180°C for five days. Product recovery (44% yield, final solution pH 2.00) led to a majority phase of platy $BaMoO_3SeO_3$ single crystals, accompanied by triangular rods (~0.05 × 0.05 × 0.3 mm) of $BaMo_2O_5(SeO_3)_2$ and microcrystalline powder.

[1] Present address: Department of Chemistry, University of Australia, Nedlands, WA 6907, Australia.

[2] Author to whom correspondence is to be addressed.

0022-4596/96 $18.00

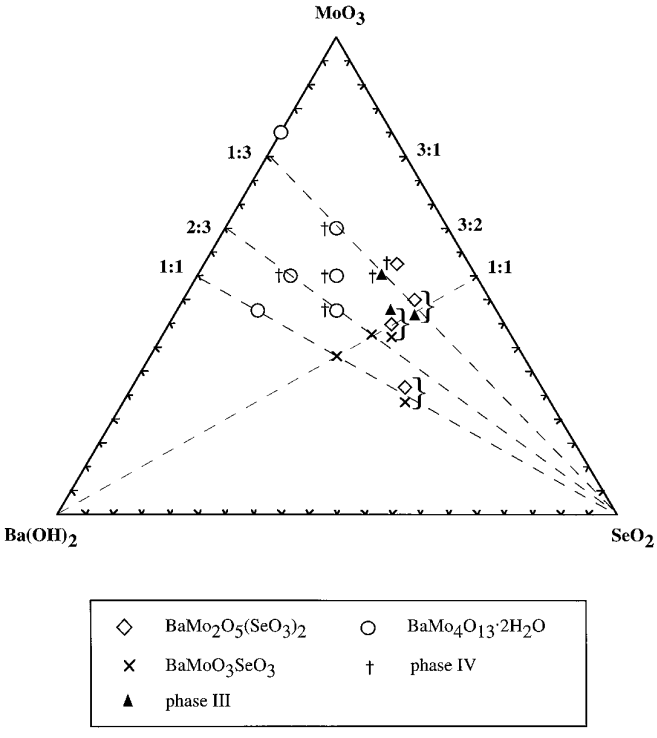

FIG. 1. Three-component mixture diagram for $BaO/MoO_3/SeO_2$, showing the relationship between reaction mixing ratios and the identities of the solid phases produced. The reaction temperature for all syntheses shown is 160°C; the final pH range for all reactions 2–3. Note that this is not a phase diagram for the Ba/Mo/Se/O system, but a representation of the solid phases recovered and identified at these sampling points under these specific preparation conditions.

A stoichiometric reaction for $BaMo_2O_5(SeO_3)_2$ (starting Ba : Mo : Se ratio = 1 : 2 : 2, heat to 180°C for five days, final pH 2.00) only resulted in a ~4% yield of $BaMo_2O_5(SeO_3)_2$ and other phases. A minority phase from this reaction was isolated by hand and identified as a barium molybdenum selenite with a hexagonal unit cell (phase III, *vide infra*).

$BaMoO_3SeO_3$ forms over a fairly wide range of conditions (Fig. 1). The best crystals of $BaMoO_3SeO_3$ were formed as irregular plates in 90% yield from a stoichiometric reaction of 1.315 g $Ba(OH)_2 \cdot 8H_2O$ (4.168 mmol Ba), 0.60 g MoO_3 (4.168 mmol Mo), 0.4625 g SeO_2 (4.168 mmol Se), and 10 cm^3 H_2O. Heating this mixture to 180°C for four days, followed by solid product recovery (final solution pH 2.6) led to the crystalline product. Synthesis at lower temperatures led to slightly increased yields of $BaMoO_3SeO_3$ (e.g., 96% yield after four-day reaction at 160°C, final solution pH 2.7).

A reaction starting from a 1 : 3 : 2 Ba : Mo : Se ratio proceeded from 0.4382 g $Ba(OH)_2 \cdot 8H_2O$ (1.389 mmol Ba), 0.60 g MoO_3 (4.168 g Mo), 0.3083 g SeO_2 (2.779 mmol Se), and 10 cm^3 H_2O. Heating this mixture to 160°C for three days resulted in a substantial yield of clear hexagonal prisms of phase III, accompanied by a second barium molybdenum selenite (phase IV) in the form of a yellow powder. Sonicating the mixture of crystals and powder in water for 15 minutes, followed by sieving (80/120 mesh sieves) recovered pure phase III. Phase IV is also produced under other reaction conditions (see Fig. 1).

Synthesis at the Ba : Mo : Se ratio (1 : 3 : 1) led only to the layered barium molybdate hydrate, $BaMo_4O_{13} \cdot 2H_2O$, as described previously (10).

Initial Characterization

The initial characterization of reaction products was by powder X-ray diffraction (Scintag XDS 2000 automated powder diffractometer, Cu$K\alpha$ radiation, λ = 1.54178 Å, T = 25(2)°C). Where possible, crystals were hand sorted by their morphologies and thoroughly ground prior to X-ray analysis. The instrumental $K\alpha 1/\alpha 2$ profile was reduced to a single $K\alpha 1$ peak position (λ = 1.540568 Å) by a software "stripping" routine, and d spacings were established relative to this wavelength. Indexing and least-squares refinement of lattice parameters was accomplished with the program TREOR (11). LAZY-PULVERIX (12) simulations based on the single-crystal structures of $BaMoO_3SeO_3$ and $BaMo_2O_5(SeO_3)_2$ were in good agreement with the observed powder patterns. For phase III, final refined hexagonal cell parameters of a = 13.0286(9) Å and c = 13.890(1) Å (V = 2042 $Å^3$) were obtained. The d-spacings, indices, and relative intensities for the three strongest peaks of phase III are d(obs) = 3.307 Å, hkl = 302, I(rel) = 100; 3.631 Å, 301, 66; 3.472 Å, 004, 76. A reasonable fit to a hexagonal unit cell (a = 12.933 (3) Å, c = 7.824 (2) Å, V = 1133 $Å^3$) was achieved using TREOR for the yellow Ba/Mo/Se/O powder (phase IV) noted above. The d-spacings, indices and relative intensities for the three strongest peaks of phase IV are d(obs) = 11.195 Å, hkl = 100, I(rel) = 100; 3.909 Å, 002, 97; 3.107 Å, 310, 95.

Infrared spectra for $BaMoO_3SeO_3$ and $BaMo_2O_5(SeO_3)_2$ (KBr pellet method) were recorded between 400 and 4000 sm^{-1} on a Galaxy FTIR 5000 series spectrometer. Thermogravimetric analysis (ramp at 5°C/min to 500°C in flowing O_2 atmosphere) was carried out on a DuPont 2950 instrument. The post-TGA residues were examined by powder X-ray diffraction.

Crystal Structure Determinations

The crystal structure of $BaMoO_3SeO_3$ was determined from single-crystal X-ray diffraction data. A transparent, irregular plate, dimensions ~0.05 × 0.25 × 0.45 mm, was mounted on a thin glass fiber with cyanoacrylate adhesive, and room-temperature [25(2)°C] intensity data were collected on an Enraf-Nonius CAD4 automated four-circle diffractometer (graphite-monochromated Mo$K\alpha$ radiation, λ = 0.71073 Å).

TABLE 1
Crystallographic Parameters for $BaMoO_3SeO_3$ and $BaMo_2O_5(SeO_3)_2$

Empirical formula:	$BaMoSeO_6$	$BaMo_2Se_2O_{11}$
Formula wt	408.23	663.13
Habit	Transparent plate	Transparent rod
Crystal system	Monoclinic	Orthorhombic
a(Å)	6.242(3)	15.883(4)
b(Å)	10.192(3)	7.887(2)
c (Å)	8.373(2)	7.780(2)
β(°)	94.94(3)	
V(Å^3)	530.6(3)	974.5(4)
Z	4	4
Space group	$P2_1/c$ (No. 14)	$Cmc2_1$ (No. 36)
T(°C)	25(2)	25(2)
λ(Mo$K\alpha$)(Å)	0.71073	0.71073
ρ_{calc} (g/cm^3)	5.11	4.52
μ(Mo$K\alpha$)(cm^{-1})	164.4	139.2
Min., max. $\Delta\rho$(e/Å^3)	−1.3, +1.3	−1.6, +1.1
Observed data[a]	1653	943
Parameters	83	78
$R(F)$[b](%)	2.87	2.22
$R_w(F)$[c](%)	3.82	2.65

[a] $I > 3\sigma(I)$ after data merging.
[b] $R = 100 \times \Sigma \|\|F_o| - |F_c\|/\Sigma|F_o|$.
[c] $R_w = 100 \times [\Sigma w(|F_o| - |F_c|)^2/\Sigma w|F_o|^2]^{1/2}$ with $w_i = 1/\sigma_i^2$.

After 25 strong reflections were located and centered, the unit cell and orientation matrix were established and optimized by least-squares refinement, resulting in the monoclinic cell parameters listed in Table 1. Excluding intensity standards, 2032 reflections were scanned ($1° < 2\theta < 65°$; $+h$, $+k$, $\pm l$). The systematic absence conditions in the reduced data ($h0l$, $l \neq 2n$; $0k0$, $k \neq 2n$) uniquely indicated space group $P2_1/c$ (No. 14). An empirical absorption correction based on ψ scans (min. = 1.76, max. = 4.21) was applied at the data reduction stage, along with the usual corrections for Lorentz and polarization effects.

The crystal structure model of $BaMoO_3SeO_3$ was solved and successfully developed in space group $P2_1/c$. Initial heavy-atom positions (Ba, Mo, Se) were located using the direct-methods program SHELXS-86 (13), and the oxygen-atom positions were easily located from Fourier difference maps. The final cycles of full-matrix least-squares refinement [program CRYSTALS (14)], using complex, neutral-atom scattering factors from the ''International Tables'' (15), minimized the function $\Sigma w_i(F_o - F_c)^2$ and included anisotropic temperature factors for all atoms and a Larson-type secondary extinction correction (16). Assuming full occupancies of all the atomic sites, the presence of Mo^{VI} and Se^{IV}, and the normal valences of Ba^{II} and O^{II} resulted in charge neutrality without any requirement for partial site occupancies or proton content, which is consistent with the spectroscopic and physical data for Ba MoO_3SeO_3 (see below). At the end of the refinement, analysis of the various trends in F_o versus F_c revealed no unusual effects. Final residuals of $R = 2.87\%$ and $R_w = 3.82\%$ were obtained for 1653 observed data [$I > 3\sigma(I)$] and 83 parameters. Crystallographic and refinement details for $BaMoO_3SeO_3$ are summarized in Table 1. Supplementary tables of anisotropic thermal factors and observed and calculated structure factors are available from the authors.

The crystal structure of $BaMo_2O_5(SeO_3)_2$ was determined in similar style, using a clear rod-like crystal ($0.1 \times 0.1 \times 0.4$ mm). A C-centered orthorhombic cell was established after completion of peak search, centering, and indexing routines (Table 1), and 1025 intensity maxima were scanned ($1° < 2\theta < 65°$; $+h$, $+k$, $+l$). The systematic absence conditions (hkl, $h + k \neq 2n$; $0kl$, $k \neq 2n$; $h0l$, h, $l \neq 2n$; $hk0$, $h + k \neq 2n$) indicated space groups $Cmc2_1$, $Cmcm$, or $C2cm$. Attempts to develop a structural model in each of these three space groups was only successful in $Cmc2_1$ (No. 36) and this space group was used for the rest of the crystallographic study. Initial heavy atom positions are from SHELXS-86; full-matrix refinement was obtained using CRYSTALS; O atoms are from difference maps; at convergence, $R = 2.22\%$, $R_w = 2.65\%$ for 78 parameters and 943 reflections with $I > 3\sigma(I)$; empirical absorption correction was obtained using DIFABS (17) [min. 0.80, max. 1.39]; the polarity of the individual crystal studied was determined by refining the Flack parameter (18) and is described below [with opposite polarity fixed, $R = 2.94\%$, $R_w = 3.26\%$]; refinement is summarized in Table 1; supplementary data (tables of anisotropic thermal factors and structure factors) are available from the authors.

Single crystals of phase III were of insufficient quality (weak scattering, very broad peak scans) to allow for single-crystal structural analysis. Phase IV could only be obtained in polycrystalline form.

RESULTS

Structure of $BaMoO_3SeO_3$

Final atomic and thermal parameters for $BaMoO_3SeO_3$ are listed in Table 2, with geometrical data given in Table 3. $BaMoO_3SeO_3$ is built up from octahedral MoO_6 and pyramidal SeO_3 groups, sharing Mo–O–Se vertices. The MoO_6 group in $BaMoO_3SeO_3$ is highly distorted, with the Mo atom displaced from the geometrical center of its six O atom neighbors by 0.41 Å. This displacement (Fig. 2) is unusual for Mo^{VI} and is locally toward an octahedral face. This results in three short Mo–O bonds [to O(1), O(2), and O(3)] with $d < 1.77$ Å, each of which is *trans* to a long [$d > 2.12$ Å] Mo–O bond [O(4), O(5), and O(6)]. The three former molybdenum–oxygen bonds are terminal, and the three latter each bridge to a different neighboring selenium atom. Despite the unusual MoO_6 distortion (*vide infra*), the bond valence sum (BVS) value

TABLE 2
Atomic Positional/Thermal Parameters for $BaMoO_3SeO$

Atom	x	y	z	U_{eq}[a]
Ba(1)	0.27121(8)	0.69135(4)	−0.01197(5)	0.0115
Mo(1)	0.7739(1)	0.92050(6)	0.23217(7)	0.0079
Se(1)	0.7094(1)	0.89852(7)	−0.17738(9)	0.0085
O(1)	0.8135(9)	1.0877(5)	0.2000(7)	0.0136
O(2)	1.0086(9)	0.8465(5)	0.1750(7)	0.0144
O(3)	0.817(1)	0.9105(6)	0.4424(7)	0.0186
O(4)	0.608(1)	0.8861(5)	0.0024(6)	0.0114
O(5)	0.4400(9)	0.9820(5)	0.2744(7)	0.0118
O(6)	0.5839(9)	0.7379(5)	0.2410(7)	0.0118

[a] $U_{eq}(Å^2) = (U_1U_2U_3)^{1/3}$.

(19) for Mo(1) is 5.96, in good agreement with the expected value of 6.00 for Mo^{VI}.

The Se(1) atom adopts the characteristic pyramidal geometry of Se^{IV} as the SeO_3^{2-} selenite anion (2). The fourth vertex about the pseudo-tetrahedral Se center is presumed to be occupied by an (unobserved) lone pair of electrons. The BVS[Se(1)] of 4.07 is in good agreement with the expected 4.00. Each Se–O vertex connects to a different nearby molybdenum atom.

The barium cation in $BaMoO_3SeO_3$ is tenfold coordinated by oxygen atoms in irregular coordination (Fig. 3). All six of the crystallographically distinct O atoms bond to Ba. The barium BVS of 1.98 is typical and a d_{av}(Ba–O) of 2.903(2) Å results. The oxygen atoms in $BaMoO_3SeO_3$ divide into two groups: O(1), O(2), and O(3) bond to Mo and Ba, and O(4), O(5), and O(6) bond to Ba, Mo, and Se.

The structural motif in $BaMoO_3SeO_3$ (Fig. 4) consists of four-rings of alternating MoO_6 and SeO_3 centers linked by Mo–O–Se bonds. These four-rings are connected into an infinite, puckered sheet of stoichiometry $[MoO_3SeO_3]^{2-}$ in the (011) plane (Fig. 5). Eight-rings (alternating Mo

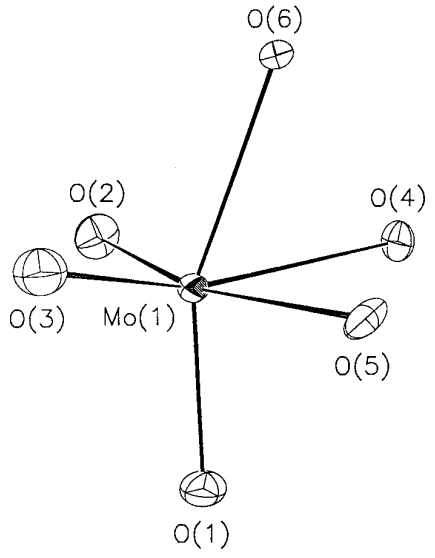

FIG. 2. ORTEP view of a detail of the $BaMoO_3SeO_3$ structure showing the distorted MoO_6 species, displaced toward the octahedral face defined by atoms O(1), O(2), O(3).

TABLE 3
Bond Distances(Å)/Angles(°) for $BaMoO_3SeO_3$

Ba(1)–O(1)	2.772(5)	Ba(1)–O(1)	2.908(6)
Ba(1)–O(2)	2.842(6)	Ba(1)–O(2)	2.995(6)
Ba(1)–O(3)	2.982(6)	Ba(1)–O(3)	3.011(7)
Ba(1)–O(4)	2.886(6)	Ba(1)–O(5)	2.785(5)
Ba(1)–O(6)	2.795(5)	Ba(1)–O(6)	3.050(6)
Mo(1)–O(1)	1.746(5)	Mo(1)–O(2)	1.750(6)
Mo(1)–O(3)	1.760(6)	Mo(1)–O(4)	2.134(5)
Mo(1)–O(5)	2.234(6)	Mo(1)–O(6)	2.211(5)
Se(1)–O(4)	1.687(6)	Se(1)–O(5)	1.698(5)
Se(1)–O(6)	1.709(5)		
O(1)–Mo(1)–O(2)	104.2(3)	O(1)–Mo(1)–O(3)	101.5(3)
O(2)–Mo(1)–O(3)	100.9(3)	O(1)–Mo(1)–O(4)	94.9(2)
O(2)–Mo(1)–O(4)	92.0(2)	O(3)–Mo(1)–O(4)	155.9(3)
O(1)–Mo(1)–O(5)	84.1(2)	O(2)–Mo(1)–O(5)	168.0(2)
O(3)–Mo(1)–O(5)	85.6(3)	O(4)–Mo(1)–O(5)	78.6(2)
O(1)–Mo(1)–O(6)	155.5(2)	O(2)–Mo(1)–O(6)	96.3(2)
O(3)–Mo(1)–O(6)	87.4(2)	O(4)–Mo(1)–O(6)	70.8(2)
O(5)–Mo(1)–O(6)	73.7(2)		
O(4)–Se(1)–O(5)	104.4(3)	O(4)–Se(1)–O(6)	95.8(3)
O(5)–Se(1)–O(6)	100.3(3)		
Mo(1)–O(4)–Se(1)	127.0(3)	Mo(1)–O(5)–Se(1)	127.4(3)
Mo(1)–O(6)–Se(1)	118.0(3)		

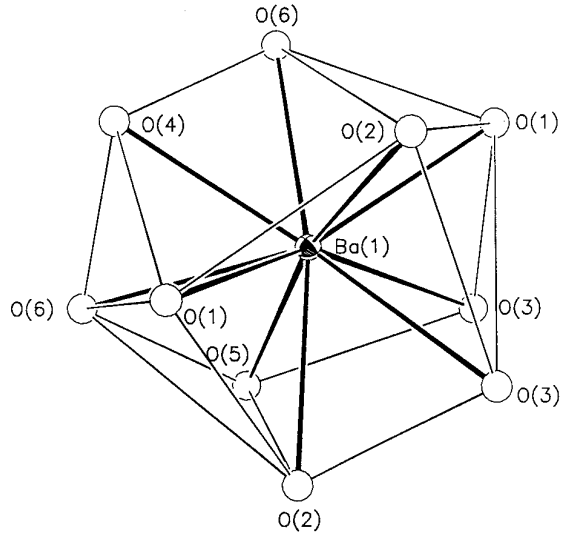

FIG. 3. Tenfold barium atom coordination in $BaMoO_3SeO_3$.

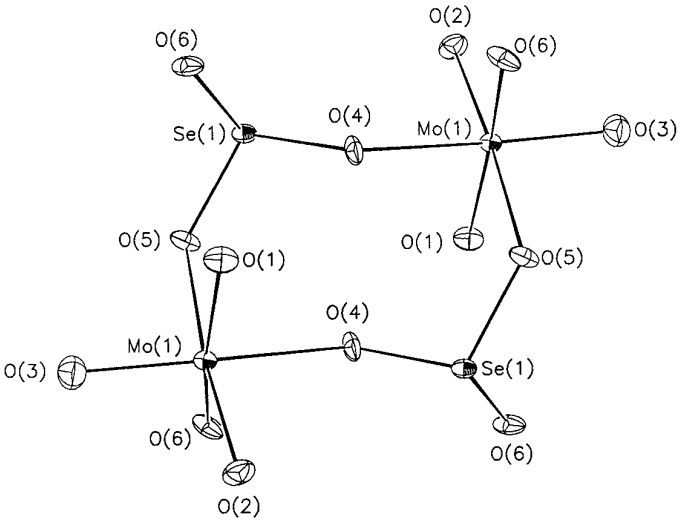

FIG. 4. Connectivity of MoO_6 and SeO_3 units into "four-rings" in $BaMoO_3SeO_3$.

and Se nodes) also result from this four-ring connectivity. Barium cations occupy sites between the Mo/Se/O layers and provide charge compensation (Fig. 6).

Structure of $BaMo_2O_5(SeO_3)_2$

Final atomic and thermal parameters for $BaMo_2O_5(SeO_3)_2$ are listed in Table 4, with geometrical data given in Table 5. $BaMo_2O_5(SeO_3)_2$ is built up from vertex-sharing MoO_6 and SeO_3 groups, connected via Mo–O–Mo and Mo–O–Se bonds, into a continuous, three-dimensional structure.

The Mo cation in $BaMo_2O_5(SeO_3)_2$ adopts a typical two short + two intermediate + two long Mo–O bond-distance distribution within the MoO_6 octahedron. The short bonds are in *cis* configuration, and each is *trans* to a long Mo–O bond. The Mo atom makes two terminal Mo=O bonds, three links to nearby Se atoms, and one link to an adjacent Mo atom [d_{av}(Mo–O) = 1.959(3) Å, BVS(Mo) = 6.00].

The Se atom [d_{av}(Se–O) = 1.699(4) Å, BVS[Se] = 4.07) in $BaMo_2O_5(SeO_3)_2$ adopts its normal pyramidal coordina-

TABLE 4
Atomic Positional/Thermal Parameters for $BaMo_2O_5(SeO_3)_2$

Atom	*x*	*y*	*z*	U^a
Ba(1)[b]	0	0.21974(9)	0.1790(1)	0.0072
Mo(1)	0.89217(4)	0.73393(8)	0.1599(1)	0.0046
Se(1)	0.79124(4)	1.0858(1)	0.3103(2)	0.0053
O(1)[b]	1	0.819(1)	0.078(1)	0.0091
O(2)	0.9102(4)	0.754(1)	0.3754(9)	0.0153
O(3)	0.9095(4)	0.5229(9)	0.126(1)	0.0135
O(4)	0.8570(3)	1.0052(8)	0.1601(9)	0.0081
O(5)	0.7648(3)	0.7214(8)	0.181(1)	0.0113
O(6)	0.8585(4)	0.7709(8)	−0.1050(8)	0.0077

[a] $U_{eq}(Å^2) = (U_1U_2U_3)^{1/3}$
[b] Wyckoff site 4*a* (symmetry m. .).

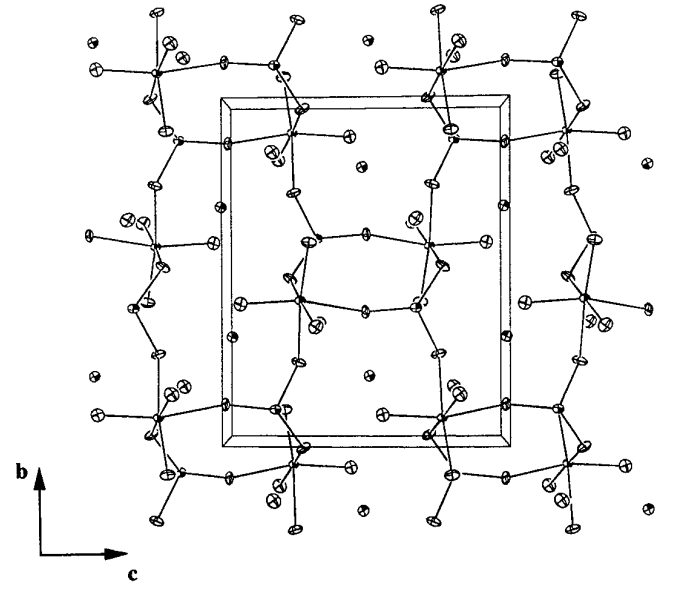

FIG. 5. View perpendicular to (011) of the $BaMoO_3SeO_3$ structure, showing the infinite network of four-rings and eight-rings built up from MoO_6 and SeO_3 units. Compare Fig. 1 of Ref. 25.

TABLE 5
Bond Distances(Å)/Angles(°) for $BaMo_2O_5(SeO_3)_2$

Ba(1)–O(1)	3.26(1)	Ba(1)–O(1)	3.122(9)
Ba(1)–O(2) × 2	2.767(7)	Ba(1)–O(3) × 2	2.820(6)
Ba(1)–O(4) × 2	2.836(6)	Ba(1)–O(6) × 2	2.807(6)
Mo(1)–O(1)	1.945(4)	Mo(1)–O(2)	1.708(7)
Mo(1)–O(3)	1.707(7)	Mo(1)–O(4)	2.211(6)
Mo(1)–O(5)	2.033(5)	Mo(1)–O(6)	2.149(6)
Se(1)–O(4)	1.691(6)	Se(1)–O(5)	1.716(7)
Se(1)–O(6)	1.689(6)		
O(1)–Mo(1)–O(2)	98.1(3)	O(1)–Mo(1)–O(3)	98.3(4)
O(2)–Mo(1)–O(3)	102.2(4)	O(1)–Mo(1)–O(4)	83.7(3)
O(2)–Mo(1)–O(4)	87.4(3)	O(3)–Mo(1)–O(4)	169.8(3)
O(1)–Mo(1)–O(5)	156.9(3)	O(2)–Mo(1)–O(5)	95.2(3)
O(3)–Mo(1)–O(5)	97.2(3)	O(4)–Mo(1)–O(5)	78.2(2)
O(1)–Mo(1)–O(6)	81.9(3)	O(2)–Mo(1)–O(6)	166.1(3)
O(3)–Mo(1)–O(6)	91.5(3)	O(4)–Mo(1)–O(6)	78.9(2)
O(5)–Mo(1)–O(6)	80.6(3)		
O(4)–Se(1)–O(5)	98.6(4)	O(4)–Se(1)–O(6)	97.5(3)
O(5)–Se(1)–O(6)	98.0(3)		
Mo(1)–O(1)–Mo(1)	123.4(5)	Mo(1)–O(4)–Se(1)	121.4(3)
Mo(1)–O(5)–Se(1)	126.4(3)	Mo(1)–O(6)–Se(1)	128.5(4)

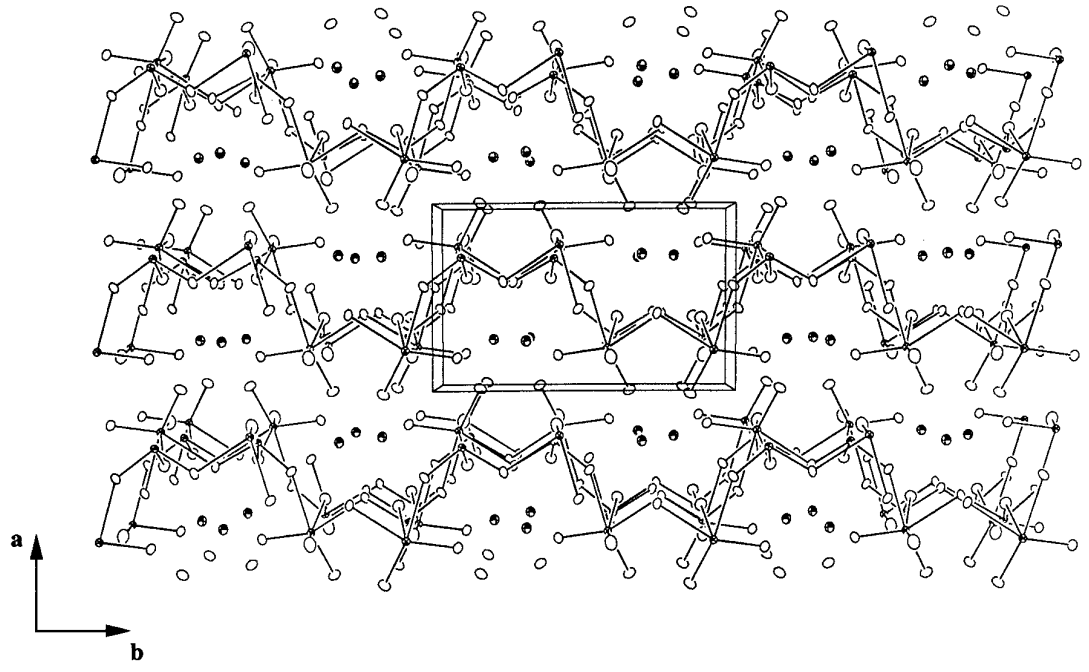

FIG. 6. View of the $BaMoO_3SeO_3$ structure perpendicular to the MoO_6SeO_3 layers. Interlayer barium cations are represented by shaded ellipsoids. Ba–O bonds are omitted for clarity.

tion for Se^{IV} (SeO_3^{2-} selenite group), and each Se–O vertex links to a different adjacent molybdenum atom. Of the six crystallographically distinct oxygen atoms, one [O(1)] links to two Mo atoms, two [O(2) and O(3)] bond only to Mo, three [O(4), O(5), and O(6)] bond to Mo and Se (Fig. 7). O(1) occupies a special position with mirror symmetry in the $BaMo_2O_5(SeO_3)_2$ structure.

The barium cation in $BaMo_2O_5(SeO_3)_2$ occupies a special position with mirror symmetry and is tenfold coordinated to nearby O atoms. All of the O atoms except O(5) participate in Ba–O bonds, resulting in d_{av}(Ba–O) = 2.884(3) Å and BVS(Ba) = 2.16. The barium coordination is distorted pentagonal prismatic (Fig. 8).

The structural motif in $BaMo_2O_5(SeO_3)$ (Fig. 9) consists

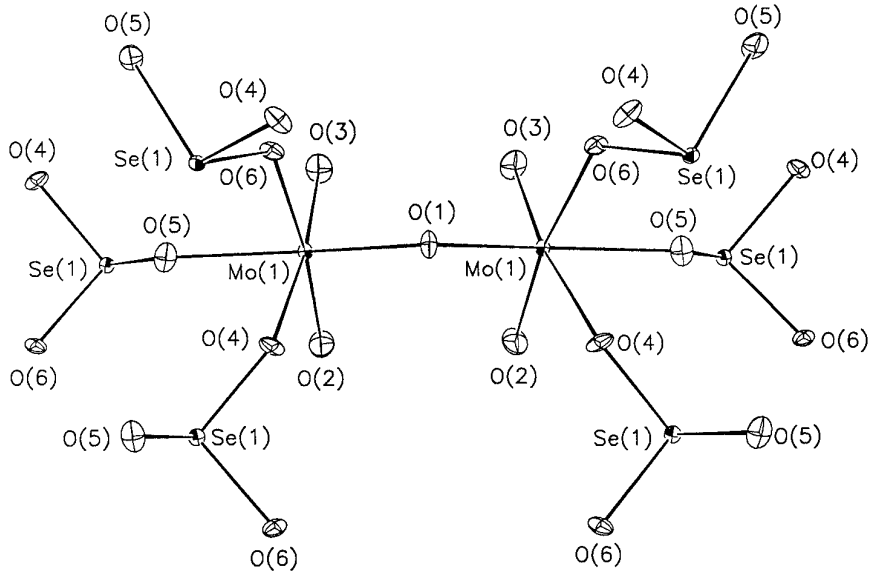

FIG. 7. View of a Mo_2O_{11} unit and surrounding selenite groups in $BaMo_2O_5(SeO_3)_2$.

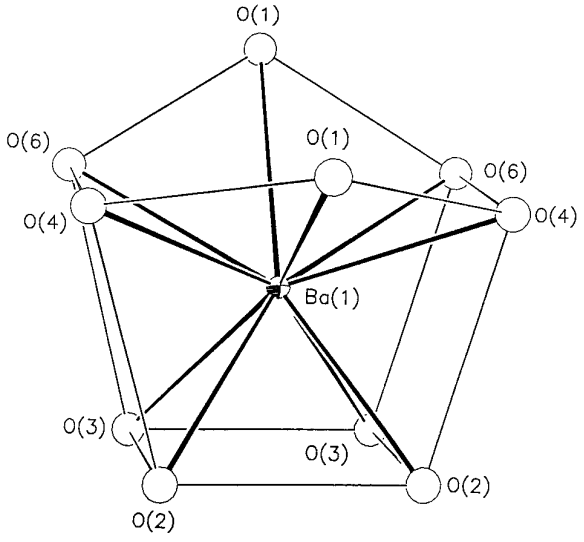

FIG. 8. Barium atom coordination in $BaMo_2O_5(SeO_3)_2$.

of pairs of vertex-sharing MoO_6 groups (i.e., Mo_2O_{11} groups), with the Mo atoms connected through O(1). Se atoms (as selenite groups) connect these Mo_2O_{11} entities into a continuous structure via Mo–O–Se bonds. The Mo_2O_{11} units are roughly aligned in the *a* direction of the unit cell, and the short molybdyl Mo=O(2) bonds are almost aligned along the polar *c* direction.

Thermogravimetric Analysis

TGA for $BaMoO_3SeO_3$ showed a sharp, one-step weight loss of 26.4% between 410 and 470°C, compared to the expected weight loss of 27.2% for the loss of one equivalent of SeO_2 from $BaMoO_3SeO_3$. Powder X-ray diffraction indicated that the post-TGA residue consisted of $BaMoO_4$ (identification by comparison with JCPDS No. 29-0193).

TGA for $BaMo_2O_5(SeO_3)_2$ showed a one-step weight loss of 31.5% from 340 to 440°C, resulting in a mixture of $BaMoO_4$ (JCPDS No. 29-0193), $BaMo_2O_7$ (JCPDS No. 34-1206), and unidentified phases. The expected weight loss for the loss of two equivalents of SeO_2 from $BaMo_2O_5(SeO_3)_2$ is 33.5%.

Spectroscopic Data

The infrared spectra of $BaMoO_3SeO_3$ (Fig. 10) and $BaMo_2O_5(SeO_3)_2$ (Fig. 11) are featureless between 4000 and 1100 cm^{-1}, which is consistent with the absence of protons in these materials (crystal structure results). Both spectra show a complex set of overlapping bands below 1000 cm^{-1}, probably due to partially resolved MoO_6 and SeO_3 modes, as previously observed in related Mo/Se/O-containing materials (2, 8).

DISCUSSION

The barium/molybdenum(VI)/selenium(IV)/oxygen phase space has been investigated by hydrothermal methods.

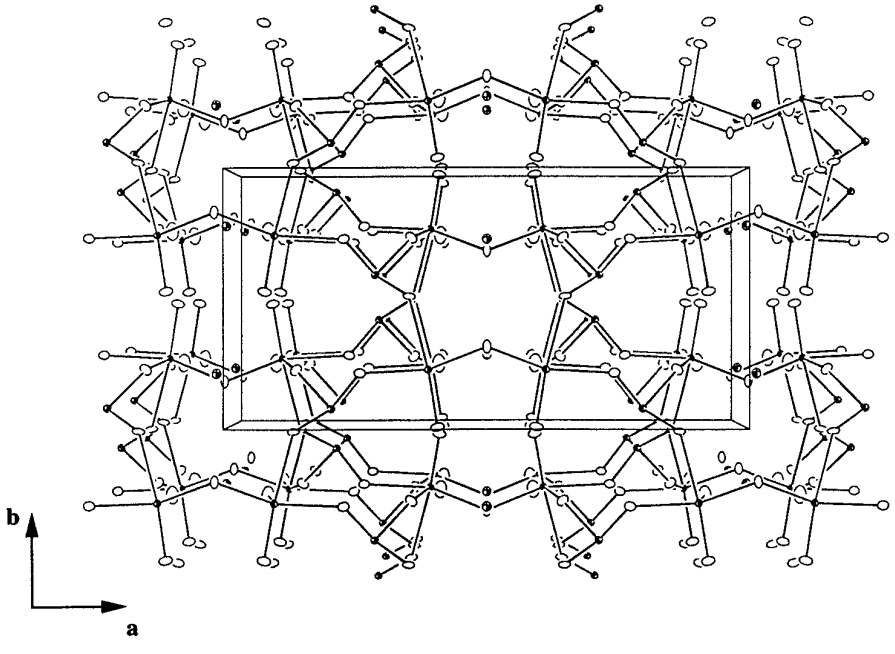

FIG. 9. View down *c* of the $BaMo_2O_5(SeO_3)_2$ structure.

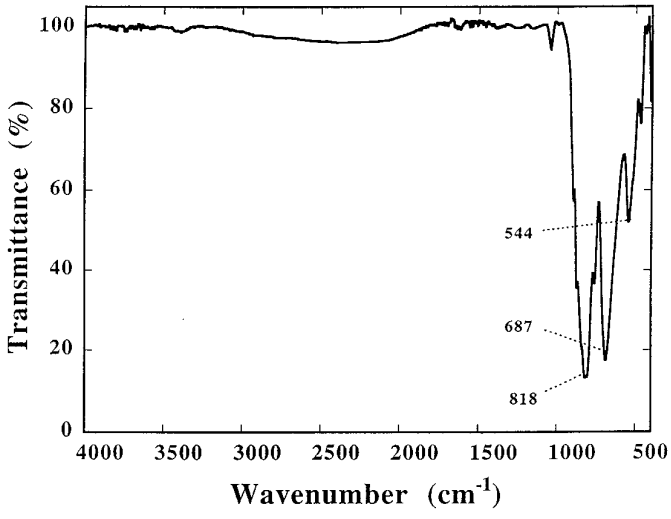

FIG. 10. IR spectrum of $BaMoO_3SeO_3$.

Four new $BaO/MoO_3/SeO_2$ phases have been identified in the region studied. The $BaO/MoO_3/SeO_2/H_2O$ phase diagram is sensitive to temperature and pH, as described in the experimental section. As is typical of hydrothermal synthesis, there is no particular correlation between ratios of the starting materials and stoichiometry of the crystalline products. $BaMoO_3SeO_3$ is formed almost quantitatively at the stoichiometric 1:1:1 Ba:Mo:Se starting ratio, but $BaMo_2O_5(SeO_3)_2$ only forms in <5% yield at a 1:2:2 Ba:Mo:Se under the heating and pH conditions investigated here. Thus, although hydrothermal methods are an outstanding route to single crystals of new materials (20), there is often little control over product composition, at least in terms of reaction composition. Exploratory synthesis, investigating a wide range of conditions (reactant ratios, concentrations, pH, and temperature) is essential to map out phases accessible by the hydrothermal method. The important role of "structure directing" agents essential to the reaction, but not incorporated into the condensed, crystalline products, has been noted previously (21).

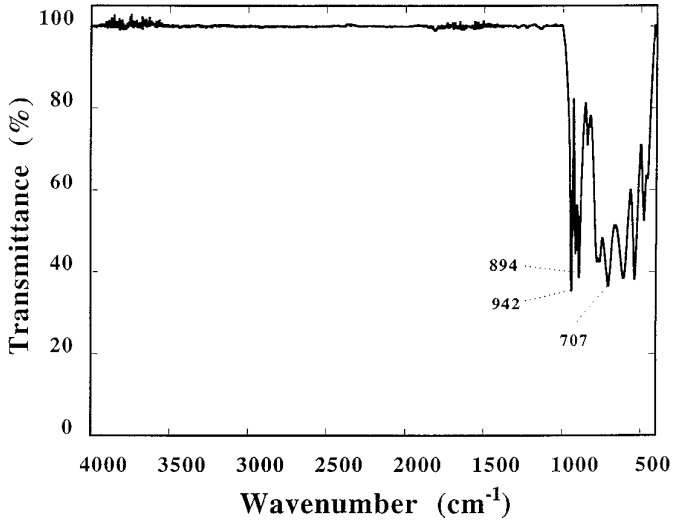

FIG. 11. IR spectrum of $BaMo_2O_5(SeO_3)_2$.

The two-dimensional $BaMoO_3SeO_3$ and three-dimensional $BaMo_2O_5(SeO_3)_2$ have been structurally characterized by single-crystal methods. The structures of these new materials are understandable in terms of the sole presence of Mo^{VI} and Se^{IV} species along with Ba^{II} and O^{II-}. They are both anhydrous despite their hydrothermal syntheses. Their spectroscopic and TGA properties are consistent with their crystal structures. In $BaMoO_3SeO_3$, the Mo atom shows an unusual displacement within its MoO_6 octahedron (three short + three long Mo–O bonds), whereas in $BaMo_2O_5(SeO_3)_2$, the MoO_6 group shows a two short + two intermediate + two long Mo–O bond-distance distribution. The structures and precise compositions of phases III and IV are at present unknown, and are being studied further.

The distortion (off-center cation displacement) of a formal d^0 cation such as Mo^{VI} in octahedral coordination may be understood in terms of a second-order Jahn–Teller effect (22). "Spontaneous" distortion of the MoO_6 group will remove (near) degeneracies in the molecular energy levels which arise from overlap of the unoccupied *d* orbitals of the metal species with the filled *p* orbitals of the oxygen atom species. The magnitude and direction of the cation displacement inside its octahedron is much harder to predict from first principles and reflects a combination of factors including second-order electronic effects, lattice stresses, and cation–cation repulsions (23). The MoO_6 group may distort in various ways: for example, in Keggin-ion structures such as $[N_2C_4H_{12}]_3Mo_{12}PO_{40}$ (24), the local distortion mode for Mo is along a Mo–O bond axis, resulting in one short Mo=O link *trans* to a long Mo–O bond and four Mo–O bonds of intermediate length. In most Mo^{VI}-containing materials, including $Ba Mo_2O_5(SeO_3)_2$, the Mo atom shifts from the nominal center of its octahedron towards an octahedral edge, resulting in two short Mo–O bonds in *cis* configuration (often described as "molybdyl" Mo=O double bonds), each of which is *trans* to a long Mo–O bond. The two remaining Mo–O vertices are of intermediate length. The third distortion mode for the Mo atom is toward an octahedral face, which results in the three short + three long Mo–O bond-distance distribution seen in $BaMoO_3SeO_3$. This third mode of octahedral distortion is uncommon, but it is also observed for the Mo species in the layered $M_2(MoO)_3SeO_3$ ($M = NH_4$, Cs) phases (2).

In $BaMoO_3SeO_3$, the three short + three long MoO_6 distortion is clearly related to the local bonding environment of the molybdenum–oxygen octahedron, with the

three long Mo–O vertices linked to nearby selenium atoms and three short Mo=O terminal vertices. The recently described isostructural layered phases $M\text{Mo}(\text{H}_2\text{O})\text{O}_2\text{PO}_4$ (M = K, NH_4) (25) show a striking resemblance to Ba MoO_3SeO_3. The $M\text{Mo}(\text{H}_2\text{O})\text{O}_2\text{PO}_4$ materials show a four-ring/eight-ring sheet structure (built up from vertex-sharing MoO_6 octahedra and PO_4 tetrahedra, with one terminal P–O bond) similar to the $\text{MoO}_6/\text{SeO}_3$ layers in Ba MoO_3SeO_3, although in the former structure type, the layers are much less puckered than the similar Mo/Se/O layers in $\text{BaMoO}_3\text{SeO}_3$. We note that in the $M\text{Mo}(\text{H}_2\text{O})\text{O}_2\text{PO}_4$ phases, the MoO_6 group shows a two short + two intermediate + two long Mo–O bond-distance distribution [two Mo=O; one $\text{Mo}-\text{OH}_2$ and one $\text{Mo}-\text{O}_\text{P}$; two $\text{Mo}-\text{O}_\text{P}$ bonds), as opposed to the three short + three long Mo–O distribution observed in $\text{BaMoO}_3\text{SeO}_3$.

ACKNOWLEDGMENTS

We thank the National Science Foundation (DMR-9214804) and the Robert A. Welch Foundation for financial support.

REFERENCES

1. J. T. Vaughey, W. T. A. Harrison, L. L. Dussack, and A. J. Jacobson, *Inorg. Chem.* **33,** 4370 (1994).
2. W. T. A. Harrison, L. L. Dussack, and A. J. Jacobson, *Inorg. Chem.* **33,** 6043 (1994).
3. W. T. A. Harrison, L. L. Dussack, and A. J. Jacobson, *Inorg. Chem.* **34,** 4774 (1995).
4. W. T. A. Harrison, L. L. Dussack, T. Vogt, and A. J. Jacobson, *J. Sol. State Chem.* **120,** 112 (1995).
5. W. T. A. Harrison, L. L. Dussack, and A. J. Jacobson, *Acta Crystallogr. C* **51,** 2473 (1995).
6. W. T. A. Harrison, L. L. Dussack, and A. J. Jacobson, *Inorg. Chem.* **35,** 1461 (1996).
7. W. T. A. Harrison, L. L. Dussack, J. T. Vaughey, and A. J. Jacobson, *J. Mater. Chem.* **6,** 81 (1996).
8. L. L. Dussack, W. T. A. Harrison, and A. J. Jacobson, *Mater. Res. Bull.* **31,** 249 (1996).
9. B. Gerand, G. Nowogrocki, J. Guenot, and M. Figlarz, *J. Sol. State Chem.* **29,** 429. (1979).
10. W. T. A. Harrison, L. L. Dussack, and A. J. Jacobson, *J. Sol. State Chem.* **116,** 95 (1995).
11. P. E. Werner, L. Eriksson, and M. J. Westdahl, *J. Appl. Crystallogr.* **18,** 364 (1987).
12. K. Yvon, W. Jeitschko, and E. Parthé, *J. Appl. Crystallogr.* **10,** 73 (1977).
13. G. M. Sheldrick, "SHELXS-86 User Guide." Crystallography Department, University of Göttingen, Germany, 1986.
14. D. J. Watkin, J. R. Carruthers, and P. W. Betteridge, "CRYSTALS User Guide." Chemical Crystallography Laboratory, Oxford University, UK, 1992.
15. "International Tables for X-Ray Crystallography," Vol. IV, Table 2.3.1. Kynoch Press, Birmingham, 1974.
16. A. C. Larson, *Acta Crystallogr.* **23,** 664 (1967).
17. N. Walker and D. Stuart. *Acta Crystallogr.* **A39,** 158 (1983).
18. H. D. Flack, *Acta Crystallogr.* **A39,** 876 (1983).
19. N. E. Brese and M. O'Keeffe, *Acta Crystallogr.* **B47,** 192 (1991).
20. M. I. Kahn and J. Zubieta, *Progr. Inorg. Chem.* **43,** 1 (1995).
21. W. T. A. Harrison, J. T. Vaughey, L. L. Dussack, A. J. Jacobson, T. E. Martin, and G. D. Stucky, *J. Sol. State Chem.* **114,** 151 (1995).
22. J. K. Burdett, "Molecular Shapes." Wiley-Interscience, New York, 1980.
23. M. Kunz and I. D. Brown, *J. Solid State Chem.* **115,** 395 (1995).
24. W. T. A. Harrison, L. L. Dussack, and A. J. Jacobson, unpublished work.
25. R. Millini and A. Carati, *J. Solid State Chem.* **118,** 153 (1995).